WeShort: Out-of-distribution Detection With Weak Shortcut structure

Jinhong Lin
University of Wisconsin-Madison
jlin398@wisc.edu

Abstract

Neural networks have achieved impressive performance for data in the distribution which is the same as the training set but can produce an overconfident incorrect result for the data these networks have never seen. Therefore, detecting whether input comes from an out-of-distribution(OOD) is key to ensuring the safety of neural networks in the real world. In this paper, we propose a simple and effective post-hoc technique, WeShort, to reduce the overconfidence of neural networks in OOD data. Our method is inspired by the observation of the internal residual structure, which shows the separation of the OOD and in-distribution (ID) data in the Shortcut. Our method is compatible with different OOD detection methods and can generalize well to different architectures of networks. We demonstrate our method in various OOD datasets to show its competitive performance and to provide reasonable hypotheses and discussions to explain why our method works. On the ImageNet benchmark, Weshort achieves state-of-the-art performance on the false positive rate (FPR95) and the area under the receiver operating characteristic (AUROC) on the family of post-hoc methods.

1. Introduction

Deep learning models achieve state-of-the-art performance in several computer vision tasks due to their effective generalization from the training data. The model is evaluated on the assumption that test data come from the same distribution as the training set. However, models deployed in the open world cannot avoid encountering new concept inputs where categories do not overlap with training data. Such a situation may lead models to produce an unrelated result to the input they have never seen and causes safety problems like autonomous driving [9] and medical diagnosis. Neural networks, for example, can produce results with high confidence. Therefore, the detection and processing of such out-of-distribution (OOD) data are critical for the practical application of deep learning models.

A straightforward idea for OOD detection is to classify data based on the confidence of the model in the input. However, deep learning models are overconfident in the OOD inputs [19], which renders it non-trivial work to depict the boundary of the OOD and ID data. As a result, the researchers propose some OOD detection methods. One is to design OOD detection oriented neural networks and objective [13] [15] [1] [11] [4] [23], which can achieve high performance OOD detection but they need overhead computation cost to retrain the models. Another one is to achieve OOD detection by applying techniques [17] [12] [16] [22] on the origin model without retraining the model nor modifying the objective. Such techniques are called post-hoc OOD detection methods, and it is easy and low cost to use in the real world. In this paper, the method we proposed is a member of the post-hoc family.

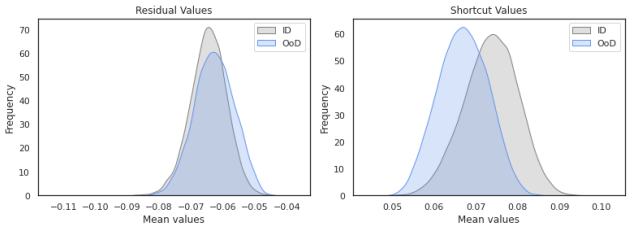

(a) Residual Values (b) Shortcut Values

Figure 1. Plots showing the distributions of the shortcut and the residuals have different separable for OOD and ID. Plot (a) demonstrates that the distribution of the residual mean values on ID (ImageNet [6]) and OOD (iNaturalist [25]); Plot (b) shows the distribution of the shortcut mean values on the above datasets.

Post-hoc OOD detection methods can be classified into two ways. On the one hand, some approaches focus on how to construct an effective measurement to classify OOD inputs. The MSP [12] achieves OOD detection by using the maximum softmax probability of the predication. The ODIN [16] increases the separation of the in-distribution (ID) and OOD data by adding small perturbations to the inputs. The energy score-based [17] detection leverages the alignment of the probability density of the inputs with the energies. On the other hand, other methods are based on the characteristics of the neural network. ReAct [22] im-

proves the OOD detection performance by removing the abnormal high activation values within the network. Our method achieves OOD detection by only modifying coefficients within the neural network, and it belongs to the latter.

In this paper, we begin with an observation in a residual structure that OOD and ID data have significant differences. Figure.1 shows the distribution of the convolution values in the middle layer of ResNet-50 trained on ImageNet. Each point on the horizontal axis corresponds to a mean of values of convolution layers on one input. Compared to values on the residual layer, the ones that exist on the shortcut layers are more distinguished from the OOD and ID data. Therefore, we put forward and examine three hypotheses in Sec.4.2. Based on assumptions, we propose a method, **We**ak **Short**cut (**WeShort**), which improves the OOD detection performance by weakening the effects of the shortcut in the residual structure as Fig.2 shows.

We examine the assumptions with extensive experiments, provide empirical insights and explain the mechanism why WeShort improves OOD detection performance. We demonstrate extensive evaluations on the common large-scale datasets to show the efficiency of our method. WeShort can be compatible with current OOD detection methods, and achieve state-of-the-art performance on various OOD detection datasets. To sum up, our key contributions are:

- We introduce WeShort, an effective and simple OOD detection approach without modifications to the trained weights. WeShort can be compatible with different OOD detection methods including MSP [12], ODIN [16], Energy score [17], ReAct [22], and generalize on various network architectures including ResNet [10] and Vision Transformer [8].
- We evaluate WeShort and demonstrate state-of-the-art performance on various OOD detection datasets and a large-scale benchmark.
- We put forward reasonable and novel hypotheses about relationships between the high and low frequency of images, neural networks, and OOD detection tasks, which could inspire future research.

We provide the outline of the paper as follows. In Section 2, we summarize the related works of the paper. In Section 3, we present the problem statement and the motivation of this paper. In Section 4, we provide the necessary preliminary hypothesis for our paper. In Section 5, we introduce our method, WeShort. In Section 6, we introduce the common datasets for OOD detection tasks, evaluate our methods and present competitive OOD detection approaches on those datasets, and explore the effects when WeShort is applied on various layers and with different σ. In Section 7, we discuss and explore why WeShort can work well via t-SNE and Eigen-CAM techniques.

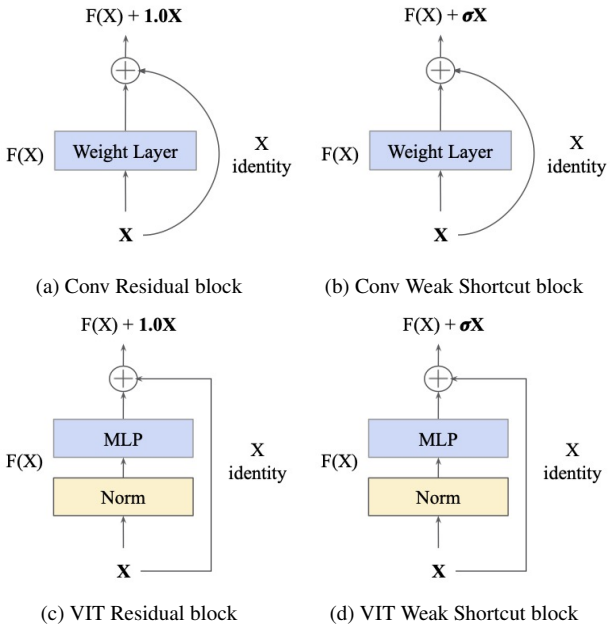

Figure 2. Plots show the difference between the residual structure and the weak shortcut structure. 2a and 2b are the blocks for ResNet-based neural networks; 2c and 2d are used for the vision transformer-based neural network. In our method, σ is always less than 1. More generally, the σ in the residual structure is 1.

2. Related Work

Post-hoc OOD detection Hendrycks and Gimpel [12] observe that a neural model tends to produce higher softmax values for ID data, and lower ones for the OOD data. Therefore, they introduce a score function, the maximum softmax probability (MSP), to achieve OOD detection. To improve the OOD detection performance, Liang [16] puts forward ODIN, which enlarges the gap between ID and OOD data by using large temperature scaling and adding perturbations on inputs. The energy-based score function is introduced by Liu [17]. Such a function gives high energy to the OOD data, and low one to the ID data. ReAct [22] exploits the characteristics of the neural network to the OOD data and leverages the OOD detection performance by removing abnormal activate values. In this paper, we investigate the impact of HFC on the OOD detection task and find out its connection with the neural network. Our method provides a novel perspective to solve the OOD detection problem, and it can be compatible with other methods to improve performance.

HFC and LFC of images Images can be decomposed into high and low frequency components (shortened as HFC

and LFC) [2] [7]. LFC contain outlines, shapes and structures of objectives, and HFC keep information edges, data distributions and noise of images [27] [3] [21]. In this paper, we explore the relationships between HFC, LFC, neural networks, and the OOD detection task. Furthermore, we exploit such connections to improve the performance of OOD detection.

Residual Structure The residual structure is proposed by [10], and it is used a lot of different fields and network architectures [14] [8] [20] [26]. In computer vision tasks, one residual structure is based on convolution neural networks as the 2a shown. Another one is based on a Vision Transformer shown on 2c. The residual structure can be viewed into two parts, one is named the Weight layer, and another one is called the Shortcut. They are shown in Fig.2c as $F(X)$ and X identity, respectively.

3. Problem Statement and Motivation

3.1. Problem Statement

In this paper, we consider the OOD detection in an image classification task. We begin to formally define the image classification problem. Consider a dataset $D_{in} := \mathcal{X}^{in} \times \mathcal{Y}^{in}$ drawn from the distribution P_{in} where P_{in} is called in-distribution, $\mathcal{X}^{in}$ denotes the in-distribution input space, $\mathcal{Y}^{in} = \{1, 2, \cdots, C\}$ is corresponding in-distribution label space, and D_{in} is named in-distribution dataset. An image classifier $\mathcal{F} : \mathcal{X} \to \mathcal{Y}$ is trained on the dataset D_{in}. More specifically, given a pair of data $\langle x, y \rangle \in \mathcal{X}^{in} \times \mathcal{Y}^{in}$, x is an image and y is its corresponding ground true label. $\mathcal{F}$ is a neural network which takes an image as an input and outputs a probability distribution P which denotes the predication of the input. Consider another dataset $D_{out} := \mathcal{X}^{out} \times \mathcal{Y}^{out}$ drawn from the distribution P_{out} where P_{out} denotes out-distribution, $\mathcal{X}^{out}$ and $\mathcal{Y}^{out}$ denote the out-distribution input space and label space. More specifically, $D_{in} \cap D_{out} = \mathcal{X}^{in} \cap \mathcal{X}^{out} = \mathcal{Y}^{in} \cap \mathcal{Y}^{out} = \varnothing$. In other words, there is no overlap of categories between D_{in} and D_{out}. The D_{out} is unreachable during the training stage of $\mathcal{F}$.

We followed the concept of the previous work [16] in our test setup to ensure fair comparative results. A new mixture distribution $P_{\mathbf{X} \times Z}$ is drawn from P_{in} and P_{out} where $Z = \{0, 1\}$and $P_{\mathbf{X} \times Z}$ indicates a conditional probability distribution. $P_{\mathbf{X}|Z=0} = P_{in}$ and $P_{\mathbf{X}|Z=1} = P_{out}$.

Based on the above settings, we are going to define an OOD detection problem. Given a mixture dataset D_m drawn from $P_{\mathbf{X} \times Z}$, OOD detection can be treated as a binary classification problem with the goal to distinguish the input data $\langle x, y \rangle \in D_m$ belonging to D_{in} or D_{out}. We can define a score function, $G(x; \mathcal{F})$, which evaluates the input x comes from which data distribution under neural network $\mathcal{F}$. Given an input x, the goal can be formulated as:

$$G(x; \mathcal{F}) = \begin{cases} 1, & \text{if } x \in D_{in} \\ 0, & \text{if } x \in D_{out} \end{cases}$$

For the post-hoc methods, most previous works [16] [12] [17]focus on designing a better score function, $G(\cdot; \cdot)$, to distinguish in- and out- distribution data. Some works [22] try to exploit the characterises of the neural network, $\mathcal{F}$, to improve the performance of OOD detection based on existing score functions. Our approach is the latter.

3.2. Motivation

Our paper is inspired by an observation that the statistical values of feature maps within a neural network are different for the ID and OOD data. Given a ResNet-50 [10], trained on ImageNet [6] and another dataset iNaturalist [25]. Since the ImageNet and iNaturalist don't overlap, which is elaborated more in 6.1.2, images in ImageNet and iNaturalist are ID- and OOD- data respectively. We gather feature maps within the ResNet-50 and calculate their mean value. More specifically, we collect outputs of the Shortcut and Weight layers on the residual structure as the description in 2 and calculate the mean values of such outputs. We can get two mean values for one input, one is from the Shortcut layer and the other one is from the Weight layer. We calculate those values in the 36^{th} layer and draw them in Fig.1. Fig.1a and Fig.1b indicate the mean values on the Weight layers and on the Shortcut respectively.

4. Preliminary and Hypothesis

4.1. Preliminary

Before exploring how HFC affects OOD detection tasks, we define some notions related to LFC and HFC, which are basically the same as [27]. The following notions are based on one channel images (Gray images) for simplifying the workload, and we only need to apply the same operations shown below on each channel of images to process RGB images. Given an image $\boldsymbol{x}$, it can be decomposed into LFC and HFC, $\boldsymbol{x} = \{\boldsymbol{x_l}, \boldsymbol{x_h}\}$ where $\boldsymbol{x_l}$ denote LFC and $\boldsymbol{x_h}$ indicate HFC. More specifically, $\boldsymbol{x}$ is transformed into a spectrum map $\boldsymbol{s}$ after the Fourier transform $\mathcal{F}(\cdot)$ as the Equ.1 shown. And the inverse Fourier transform $\mathcal{F}^{-1}(\cdot)$ can be applied on $\boldsymbol{s}$ to get $\boldsymbol{x}$ shown on the Equ.2. To simplify the problem, we only consider the real part of the Fourier transform in this paper.

$$\boldsymbol{s} = \mathcal{F}(\boldsymbol{x}) \tag{1}$$

$$\boldsymbol{x} = \mathcal{F}^{-1}(\boldsymbol{s}) \tag{2}$$

Given a spectrum map $\boldsymbol{s} \in \mathbb{R}^{n \times n}$ generated from $\boldsymbol{x} \in \mathbb{R}^{n \times n}$, the Euclidean distance function $\mathcal{D}(\cdot, \cdot)$, and a center coordinates of $\boldsymbol{s}$ is denoted as (c_i, c_j) where $c_i, c_j \in \mathbb{R}$. In

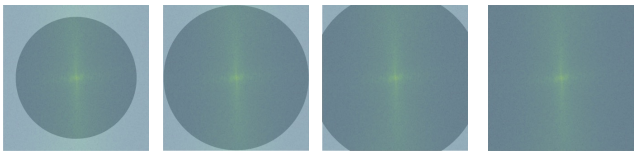

(a) R=90 (b) R=112 (c) R=130 (d) R=∞

Figure 3. Plots of various overlap examples for spectrum maps.

order to separate $\boldsymbol{x_l}$ and $\boldsymbol{x_h}$ from $\boldsymbol{x}$, $\boldsymbol{s}$ need to be split into $\boldsymbol{s_l}$ and $\boldsymbol{s_h}$ according a hyper parameter,radius R, as Equ.3 Equ.4 and Fig.3 shown. $\boldsymbol{s_l}$ and $\boldsymbol{s_h}$ indicate LFC and HFC in $\boldsymbol{s}$ respectively. Subsequently, $\mathcal{F}^{-1}$ is applied on $\boldsymbol{s_l}$ and $\boldsymbol{s_h}$ to get $\boldsymbol{x_l}$ and $\boldsymbol{x_h}$ expressed in Equ.5.

$$s_l(i,j) = \begin{cases} s(i,j) & D((i,j),(c_i,c_j)) \leq R \\ s(i,j) \times z & D((i,j),(c_i,c_j)) > R \end{cases} \tag{3}$$

$$s_h(i,j) = \begin{cases} z & D((i,j),(c_i,c_j)) \leq R \\ s(i,j) \times z & D((i,j),(c_i,c_j)) > R \end{cases} \tag{4}$$

$$\begin{aligned} \boldsymbol{x_l} &= \mathcal{F}^{-1}(\boldsymbol{s_l}) \\ \boldsymbol{x_h} &= \mathcal{F}^{-1}(\boldsymbol{s_h}) \end{aligned} \tag{5}$$

In the Equ.3 and Equ.4, z is chosen 0 or 0.5 in the following experiments. If $z = 0$, the relevant information is removed. Otherwise, the components are weakened. We illustrate different situations with various R in Fig.3. Note that all components are kept when R is ∞.

4.2. Hypothesis

Hypothesis 1 (H1): *The high-frequency components (HFC) contain some information that hurts the OOD detection performance, yet some are helpful for the OOD detection task.*

Inspired by [27] that HFC brings higher accuracy but hurts the robustness of the neural network, we assume that HFC affects the performance of the OOD detection. The following empirical results show this assumption is reasonable.

In order to examine the H1, we evaluate OOD detection performance after removing or weakening HFC of images. More specifically, HFC, $\boldsymbol{x_h}$, are removed from the image $\boldsymbol{x} = \{\boldsymbol{x_l}, \boldsymbol{x_h}\}$.Therefore, we evaluate the H1 by saving the components of spectrum maps within a circle with radius R as Fig.3 demonstrates. We conduct two experiments. The first is that z in the Equ.3 and Equ.4 are 0.5. Such an operation keeps all LFC and **weakens** HFC. The second experiment is to set z to 0 such that the HFC are totally **removed**.

		Average			
R	Overlap	FPR95↓	AUROC↑	AUPR↑	ID ACC↑
∞	1.00	57.33	87.07	97.15	**76.11**
140	0.97	57.35	87.05	97.15	**76.11**
130	0.93	57.29	87.06	97.15	76.10
120	0.86	56.98	87.11	97.16	76.02
112	0.78	56.59	87.19	97.19	75.73
100	0.63	55.39	87.31	97.22	75.05
90	0.51	55.17	**87.35**	**97.24**	74.54
80	0.40	**55.15**	87.28	97.23	73.70
70	0.31	55.21	87.15	97.21	72.97
60	0.22	56.49	86.99	97.20	72.01

Table 1. Hypothesis 1 experiments on the first experiment. The outside of the circle is filled with 0.5. R indicates the radius of the circle, as Fig.3 shows. Overlap indicates the overlap of the circle and the spectrum. A larger overlap means much high-frequency information is kept and vice versa. ↑ indicates that larger is better and ↓ indicates that smaller is better. The best performance is bold and the second best is underlined.

		Average			
R	Overlap	FPR95↓	AUROC↑	AUPR↑	ID ACC↑
∞	1.00	57.33	**87.07**	**97.15**	**76.11**
140	0.97	57.39	87.04	97.14	76.08
130	0.93	57.38	87.03	97.14	75.98
120	0.86	57.55	86.99	97.14	75.72
112	0.78	57.37	87.00	**97.15**	75.13
100	0.63	**56.75**	86.84	97.13	73.69
90	0.51	57.63	86.43	97.04	72.13
80	0.40	59.07	85.73	96.89	69.91
70	0.31	59.97	84.89	96.70	67.18
60	0.22	62.06	83.82	96.46	63.75

Table 2. Hypothesis 1 experiments on the second experiment. The outside of the circle is filled out with 1.0. All symbols are same as those on the Tab.1

The results are shown on the Table.1 and Table.2. When $z = 0.5$ i.e. to weaken HFC, we observe that the OOD detection performance increases with the number of weakened HFC yet the In-distribution accuracy decreases. Whereas, when $z = 0$ i.e. to remove HFC, the performance of OOD detection drops compared to the baseline and the ID accuracy decreases faster than when the HFC are weakened. Based on these two phenomena, we come to two conclusions. One is that HFC can help the model to improve the accuracy of the classification task. The other conclusion is that some of the information in the HFC is useful for the OOD detection task, while some of it can harm the performance of OOD detection.

Hypothesis 2: *More HFC of inputs are kept on the Shortcut than those on the Weight Layer.*

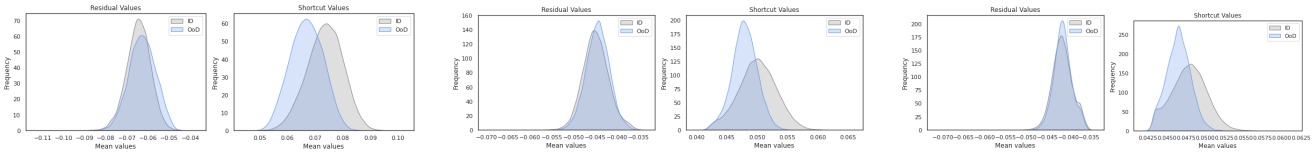

(a) R=0 (b) R=100 (c) R=110

Figure 4. The statistical values on Weight Layers (Main Values) and Shortcut (Shortcut Values).

Model	Method	iNaturalist [25]		SUN [28]		Places [29]		Textures [5]		Average	
		FPR95↓	AUROC↑	FPR95↓	AUROC↑	FPR95↓	AUROC↑	FPR95↓	AUROC↑	FPR95↓	AUROC↑
ResNet	Energy [17]	53.93	90.59	58.27	86.73	65.40	84.13	52.29	86.73	57.47	87.05
	Ours(Energy)	37.99	93.99	45.74	91.52	57.47	88.12	47.25	89.67	47.11	90.82
	MSP [12]	52.77	88.42	68.58	81.75	71.57	80.63	66.13	80.46	64.76	82.82
	Ours(MSP)	27.34	94.27	52.13	87.92	60.21	85.20	57.23	84.38	49.23	87.94
	ODIN [16]	41.46	91.37	54.08	86.89	62.12	84.44	45.55	87.56	50.80	87.57
	Ours(ODIN)	21.91	95.46	35.38	93.53	47.82	90.32	**39.13**	91.14	36.06	92.61
	ReAct [22]	19.73	96.37	23.66	94.44	33.31	91.96	46.29	90.30	30.75	93.27
	Ours(ReAct)	**15.90**	**96.92**	**19.47**	**95.94**	**31.64**	**92.67**	41.05	**92.58**	**26.50**	**94.54**
VIT	Energy [17]	37.89	94.46	69.33	84.52	72.06	82.74	52.00	88.30	57.82	87.50
	Ours (Energy)	26.11	**95.43**	**60.53**	**86.44**	**63.86**	**84.59**	**46.61**	**89.04**	**49.28**	**88.87**
	MSP [12]	39.42	92.41	73.79	79.49	74.05	79.56	63.05	81.50	62.58	83.24
	Ours (MSP)	33.10	93.25	69.94	80.43	70.37	80.45	59.33	82.48	58.18	84.15
	ODIN [16]	26.00	94.93	65.98	84.57	68.78	82.72	53.74	87.09	53.63	87.33
	Ours (ODIN)	**25.05**	94.52	60.55	85.62	64.36	83.74	49.18	87.25	49.79	87.78
	ReAct [22]	63.62	92.42	85.35	80.72	85.45	78.86	66.51	86.01	75.23	84.50
	Ours(ReAct)	49.12	93.24	78.49	82.86	79.83	80.92	61.37	86.45	67.20	85.87

Table 3. Comparison results. Comparison with the competitive out-of-distribution detection methods. All methods are based on the same weights and are only trained on the ID data (ImageNet-1k). The best performance is bold and the second best is underlined. ↑ means that larger values are better and ↓ indicates that smaller values are better.

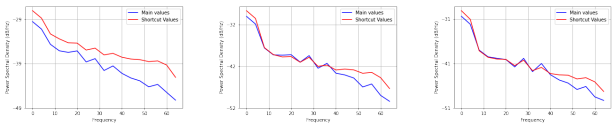

(a) R=0 (b) R=80 (c) R=100

Figure 5. The power spectral density of feature maps on Weight Layers (Main Values) and Shortcut (Shortcut Values).

Hypothesis 3: *The HFC contain information related to data distributions.*

To demonstrate the plausibility of the above two hypotheses, we conduct experiments only using the HFC. More specifically, Equ.4 is applied and $z = 0$. As R increases, more LFC are removed, and the percentage of HFC increases. When $R = 0$, the inputs are original images.

The first suit experiment is to count the mean values of feature maps when inputs with various amounts of LFC are fed into the neural network, and observe the difference between two data distributions as the amount of removed LFC increases. In our experiments, R $\in \{0, 100, 110\}$. We visualize statistical values of the weight layer and the shortcut shown on 4. We can observe that as the R grows, i.e. the number of removed LFC increases, the difference of statistics on the Shortcut for the ID- and OOD- data change dramatically compared to those on the Weight Layer.

The second suit experiment is about visualizing the power spectral density of feature maps on Weight Layers and Shortcut. The environment settings are similar to what we describe above but R $\in \{0, 80, 100\}$. As Fig.5 shows, the amount of high-frequency information on Weight Layers is larger than that on Shortcut. Therefore, we conclude the following conclusions:

1. The Shortcut contains more information from the HFC than one from the Weight Layer.

   The first evidence to prove the above statement is statistical values on the Shortcut and the Weight Layer. As R increases, the LFC of inputs from ID and OOD converge to the same, 0, which is consistent with Fig.4 that mean value distribution on the Weight Layer keeps to be closer as more LFC are removed. Whereas, the shortcut values keep differently and it is consistent with the difference in the HFC of inputs since HFC are kept. In summary, the Shortcut demonstrates distinguishing statistical values for the different HFC and the Weight Layer.

The second piece of evidence is the power spectral density of feature maps shown. To find out the connection between the HFC, LFC of inputs, and the high, and low frequency of feature maps, we visualize the change of their power spectral density (PSD) of them in Fig.5. Such a consistency implies that low and high frequencies of PSD on the feature maps are corresponding to the number of LFC and HFC of inputs. Based on this assumption, we can conclude that Shortcut contains more HFC information of inputs than that on the Weight Layer because of a larger PSD of high frequency on the Shortcut.

When more LFC of inputs are replaced with 0 i.e. R increases, the difference between low-frequency information on the Shortcut and the Weight Layer is smaller.

2. The HFC contains information related to data distributions. With more LFC removed and the percentage of HFC increased, statistical values from ID and OOD on the shortcuts change differently. As Fig.4 shows, the kurtosis for OOD is larger than that for ID as R increases, whereas they are approximately the same when R is 0. In summary, the statistical values of different data distributions are changed differently when the percentage of HFC varies.

H1 indicates that we can achieve OOD detection performance increased whereas H3 implies that some information on HFC can help us to classify them well. A straightforward idea is to disentangle them to exploit useful formation for OOD detection tasks. However, it is hard for us to do that [27]. The results when removing and weakening HFC in Tab.1 and 2 inspire us to weaken HFC instead of ignoring them is a good approach.

Due to H.3, we can weaken HFC by placing a small weight on the Shortcut. LFC are important and hold higher priority for learning of neural networks [27], and H.2 indicates LFC are kept on the Weight Layer mostly. Therefore, we conclude that OOD detection performance can be improved by weakening the Shortcut and keeping the Weight Layer as normal. Based on such a conclusion, we put forward our method, WeShort.

5. Method

The analysis of the previous sections suggests that a very simple change to the Residual Structure can help to distinguish in-distribution from out-distributional data, and then we introduce a simple and effective OOD detection method, **We**ak **Short**cut (WeShort).

Based on the H3, the key idea to improve the OOD detection performance is to weaken the effects that the shortcut brings. Specifically, we denote an output of a pre-trained neural network residual structure as $F(x) + x$, where x denotes the feature map and F denotes the Weight Layer in the Convolutional Neural Network or Norm and MLP in the Vision Transformer network as the Fig.2 shows.

	Average			
σ	FPR95 ↓	AUROC ↑	AUPR ↑	ID ACC ↑
1.000	30.70	93.30	98.59	<u>74.87</u>
0.975	28.62	93.84	98.70	**74.95**
0.950	<u>26.73</u>	94.35	98.82	74.39
0.925	**26.50**	**94.54**	<u>98.87</u>	73.10
0.900	26.99	<u>94.54</u>	**98.89**	71.08
0.875	28.58	94.27	98.85	67.79
0.850	30.47	93.75	98.76	62.65
0.825	33.50	92.93	98.60	54.79
0.800	39.60	91.72	98.36	44.06

Table 4. Shortcut Impact Table. σ indicates the strength of the impact from the Shortcut. Larger value of σ indicates larger impact from the shortcut. FPR95, AUROC and AUPR are explained in the 6.3. ID ACC indicates the accuracy of the model to the In distribution data. ↑ indicates that larger is better and ↓ indicates that smaller is better. Best performance is bold and the second best is underlined.

WeShort: Weak Shortcut We propose the WeShort operation, which is applied on the residual structure of the neural network. In order de
The origin residual structure:

$$\hat{y}_o = F(x) + x \tag{6}$$

The weak shortcut structure:

$$\hat{y}_s = F(x) + \boldsymbol{\sigma} x \tag{7}$$

Where $\hat{y}_o$ and $\hat{y}_s$ indicate the output of the residual structures and the weak shortcut structure respectively. $\boldsymbol{\sigma}$ is a coefficient used to control how weak that the shortcut brings.

When $\boldsymbol{\sigma}$ is 1, the WeShort degenerates to the origin residual structure. Since my goal is to reduce the effect of the shortcut, $\boldsymbol{\sigma}$ is always less than 1. When $\boldsymbol{\sigma}$ is 0, it means that the effect of the shortcut is ignored and the output is depended on the $F(x)$.

6. Experiments

In this section, we not only evaluate the effectiveness of our method, but also demonstrate the reasonableness of the assumptions. We evaluate WeShort on a OOD detection benchmark (ImageNet [6]) to show its effectiveness and then exemplify the assumptions by extensive experiments on the ImageNet [6] and iNaturalist [25] datasets.

(a) ImageNet-1k [6] (b) iNaturalist [25] (c) SUN [28] (d) Places [29] (e) Textures [5]

Figure 6. We list images of ImageNet-1k and various OOD datasets, which is descried in the Section 6.1

6.1. Datasets

We illustrate some samples from datasets in Fig.6.

6.1.1 ID dataset

We use pre-trained ResNet50 [10] and Vision Transformer [8] for ImageNet-1k [6]. The dataset contains 1000 classes covering a wide range of objects. Compared to the small resolution datasets, CIFAR (32x32) and TinyImageNet (36x36), the size of the images in the ImageNet is 224x224, which is closer to the real-world.

6.1.2 OOD dataset

We evaluate the OOD detection performance on the high resolution datasets, which cover different scenes containing plants, animals, natural objects, textrual images. Note that there is no overlap between classes between the ID data and the OOD data, and it is same as the MOS does.

iNaturalist [25] iNaturalist dataset contains 5,000 categories of plants and animals 800x800 images. 110 different classes of images are picked up that don't overlap with ones in ImageNet-1k, and 10,000 images are selected randomly.

SUN [28] SUN dataset contains 397 classes of natural images that are larger than 200x200 resolutions. 10,000 images are selected randomly over those 50 classes, and there are no overlap categories with ones in ImageNet-1k.

Places [29] Places dataset contains 205 categories of scene images whose resolution are layer 512x512. 50 different classes of 10,000 images are picked up that don't overlap with ones in ImageNet-1k.

Textures [5] Textures dataset contains 47 classes of textural images whose resolutions are either 300x300 or 640x640. The whole datasets containing 5,640 images are used for evaluation.

Model	Method	Average		Δ	
		FPR95↓	AUROC ↑	FPR95 ↑	AUROC ↑
ResNet	Energy [17]	57.47	87.05	10.36	3.77
	Ours(Energy)	47.11	90.82		
	MSP [12]	64.76	82.82	15.53	5.12
	Ours(MSP)	49.23	87.94		
	ODIN [16]	50.80	87.57	14.74	5.04
	Ours(ODIN)	36.06	92.61		
	ReAct [22]	30.75	93.27	4.25	1.27
	Ours(ReAct)	26.50	94.54		
VIT	Energy [17]	57.82	87.50	8.54	1.37
	Ours (Energy)	49.28	88.87		
	MSP [12]	62.58	83.24	4.40	0.91
	Ours (MSP)	58.18	84.15		
	ODIN [16]	53.63	87.33	3.84	0.45
	Ours (ODIN)	49.79	87.78		
	ReAct [22]	75.23	84.50	8.03	1.37
	Ours(ReAct)	67.20	85.87		
Average Improvement		\	\	8.58	2.36

Table 5. Improvement result. The table shows the improvement that our method brings based on the existing methods. Δ indicates how much improvement of performance that WeShort increases. ↑ indicates that larger is better and ↓ indicates that smaller is better. Specifically, larger values indicate more improvement brought by WeShort in the Δ columns.

We evaluate a suite of OOD detection methods and WeShort on ImageNet

6.2. Implement details

We use a pretrained ResNet50 [10] and Vision Transformer [8] for ImageNet-1k [6]. We evaluate a suite of OOD detection methods and WeShort on ImageNet [6], iNaturalist [25], SUN [28], Places365 [29], and Textures [5], where the first dataset is ID data and the rest of them are OOD data. All images are resized to 224x224 before they are fed into the neural network. All experiments are finished on the GeForce GTX 1080 Ti. Our code is based on ReAct [22].

6.3. Evaluation Metrics

We evaluate the common and our OOD detection method on the following two metrics:

Block Index	Average			
	FPR95↓	AUROC ↑	AUPR ↑	ID ACC ↑
Baseline	30.70	93.30	98.59	74.87
1	32.87	92.88	98.51	73.45
2	29.25	93.64	98.67	72.73
3	26.50	94.54	98.87	73.10
4	30.32	93.37	98.61	74.86

Table 6. Blocks Impact Result. The column of Block Index indicates which residual block is selected to apply WeShort. The first row (Baseline) indicates WeShort does not apply to the model. ↑ indicates that larger is better and ↓ indicates that smaller is better.

FPR95 FPR95 measures the FPR (False Positive Rate) of the OOD data when the recall (Positive Rate of the ID data) is at 95%. More specifically, a lower FPR95 indicates better performance of OOD detection.

AUROC AUROC measures the area under the TPR (True Positive Rate) and FPR (False Positive Rate). More specifically, a higher AUROC indicates better performance of OOD detection.

AUPR AUPR indicates the area under the precision-recall curve. A higher AUPR is better.

6.4. Result

6.4.1 WeShort vs. Existing Methods

The main result of our comparison with the commonly post-hoc OOD detection methods is in Table.3. For fair evaluation, all the experiments are conducted under the same network weights and backbone without reaching out any OOD data during the training stage. As the Table.3 shown, the results with gray background color are our methods, and ones with white background color are the existing methods. Our method outperforms than all baselines. In order to compare the result and the improvements easily, we report the improvement brought by the WeShort based on the existing methods in the Table.5. Under same weights and score functions, our method leverage the average performance by 8.58% in FPR95.

6.4.2 WeShort with Different Degree Impact from the Shortcut

As the Section.5 explained, the degree of impact from the shortcut is determined by the σ. Larger σ indicates more impact from the shortcut, and vice versa. We conduct experiments to various $\sigma \in \{1, 0.975, 0.95, 0.925, 0.90, 0.875, 0.85, 0.825, 0.80\}$ on the same blocks based on the ReAct with ResNet architecture. The results of experiments

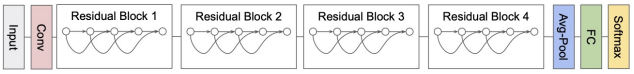

Figure 7. The plot shows an architecture of ResNet50

are listed in the Table.4. We observe that the OOD detection performance increases as σ decreases before reaching out 0.925. The detection performance decreases after σ is 0.925 while they are still better than the baseline (σ is 1) before it is 0.85. In general, the ID accuracy (ID ACC) decreases as the σ decreases, but it is still in an acceptable range. However, an interesting phenomenon is that the ID ACC increases when the σ is at 0.975 compared to the one when σ is 1.0.

6.4.3 WeShort on Different Blocks

The neural network can be divided into multiple blocks as Fig.7 shows. In this subsection, we explore the OOD detection performance when we apply WeShort on different blocks of the neural network. All experiments are conducted on the ResNet50 [10] and σ is 0.925. The results are shown in the Table.6. We observe that the OOD detection performance drops when the WeShort applies on shallow layers, but performance is improved while it works on the deeper blocks. We observe that the OOD detection performance drops when the WeShort applies on shallow layers, but performance is improved while it works on the deeper blocks. We conclude the reason behind it is that the shallow blocks mainly capture the general features without relating to the data distribution.

7. Discussion

In this section, we are going to discuss why WeShort can work well. We will visualize the class activation map on Weight layers and Shortcuts respectively to understand what do they learn, and thus further to explain how can WeShort work.

7.1. What do neural networks learn on Weight layers and Shortcuts?

Since the key to WeShort is to mitigate the impact of shortcuts, we first need to understand the impact of shortcuts. We visualize the CAM on Weight layers and Shortcuts via Eigen-CAM [18] technique.

We randomly select images from ID- and OOD- datasets as section.6.1 describes. As shown in the figure.8, the features captured by the Weight Layer are more specific to the object, yet the Shortcut has a larger perception. In other words, the Weight Layer focuses more on the important regions (classification task-relevant regions) and the size of such regions is smaller than that captured by the Shortcut.

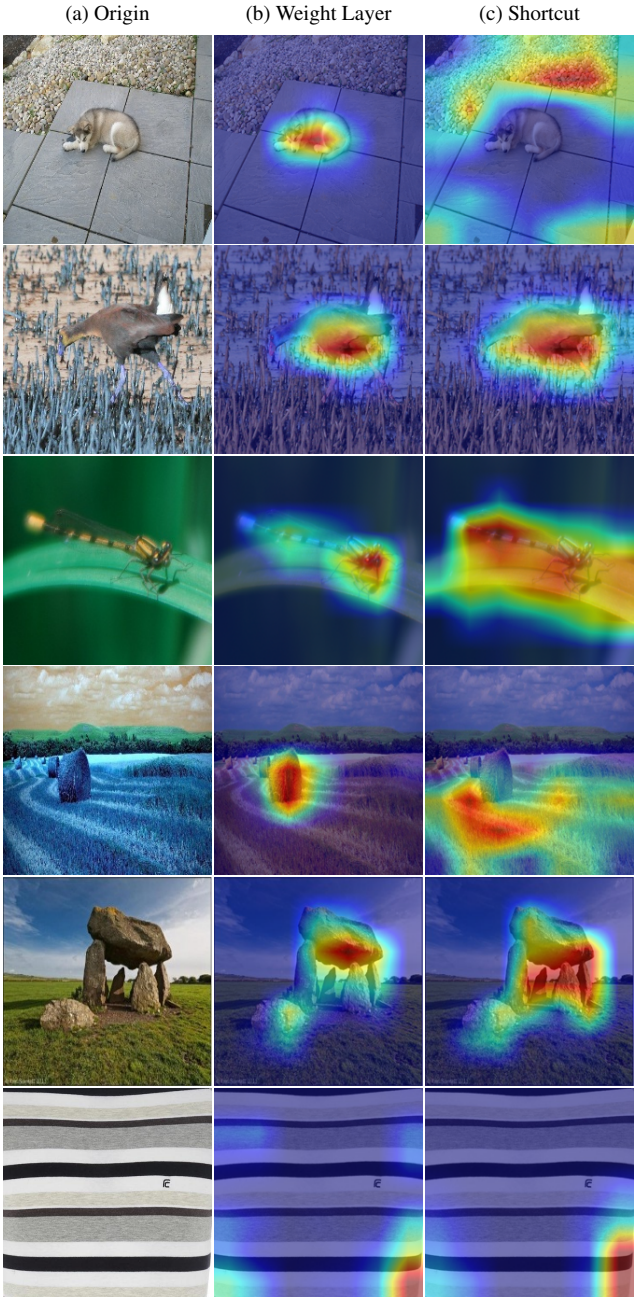

Figure 8. Visualization with Eigen-CAM. The first column represents the origin images, the second column shows the CAM on the weight Layer, and the third column is the CAM on the Shortcut.

Therefore, we conclude that the Weight Layer is more conservative than the Shortcut.

7.2. Why does the WeShort do well?

Such features are useful for OOD detection tasks. The image classification task can be viewed as extracting features from an image and finding the most relevant classes

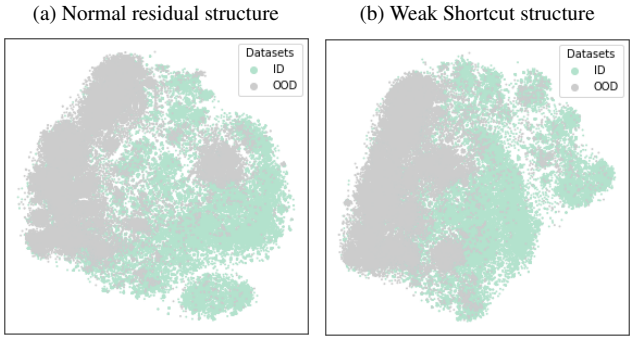

Figure 9. The Feature Distribution. It is drawn with t-SNE [24]. ID indicates ImageNet dataset [6]. OOD indicates iNaturalist [25], SUN [28], Places [29] and Textures [5]

from a limited number of options. For example, given an image and a model trained on a 1000-class dataset, the goal of the classification task is to find the category that is most similar to the given image. Therefore, relevant features on a given image contribute to the model's correct prediction. However, such a characteristic may hurt OOD detection performance. Since the model finds the most similar category according to features extracted from a given image, weakly correlated or uncorrelated features in the image may convince the model to output a high confidence score. In the OOD detection task, these characteristics may lead to higher predictive scores for the OOD data in models.

As shown in Fig.8, weak or irrelevant features are mainly captured by the Shortcut. So, by diluting the impact of shortcuts, the model becomes less sensitive to these features, which is what WeShort does.

7.3. Features space distribution

In this subsection, we will draw the features of ID- and OOD- datasets extracted by the normal residual structure2a and Weak Shortcut structures2b. As 9 shows, features extracted by the Weak Shortcut structure are more separable between ID- and OOD- data. Another important observation is that the feature distances from the Weak Shortcut structure are more closer. Such features reduce the complexity of the decision boundaries for classifying ID- and OOD-data,. We conclude that, for the same reason as shown in Fig.reffig:CAM, the weakly correlated features are weakened and thus the features used for the same category are more similar. More specifically, since the weakly relevant features, such as the water and land backgrounds in the boat images, are weakened, the main feature that contributes to the final classification is the boat itself. As a result, their similarity increases.

7.4. Mathematical Analysis

Since the multiple convolutional layer is non-linear filters, it is hard to prove it is high or low pass directly. We assume it is low pass via the experience results Fig.5.

8. Conclusion

In this paper, we provide a simple OOD detection method, WeShort, which attenuates the effect of the Shortcut on residual structures during OOD detection. We provide and examine reasonable hypotheses about the relationship between HFC and LFC of images, the deep learning model, and the OOD detection task. Based on such hypotheses, we achieve the improvement of OOD detection by decreasing the effect of the Shortcut. Extensive experiments on the ImageNet and large-scale OOD datasets show that WeShort can improve OOD detection on various neural network structures including the Convolution-based and Vision Transformer-based neural networks. We also discuss why WeShort works well with t-SNE technology the t-SNE technique Class Activation Mapping and feature mapping.

References

[1] Julian Bitterwolf, Alexander Meinke, and Matthias Hein. Certifiably adversarially robust detection of out-of-distribution data. *Advances in Neural Information Processing Systems*, 33:16085–16095, 2020. 1

[2] Fergus W Campbell and John G Robson. Application of fourier analysis to the visibility of gratings. *The Journal of physiology*, 197(3):551, 1968. 3

[3] Yunpeng Chen, Haoqi Fan, Bing Xu, Zhicheng Yan, Yannis Kalantidis, Marcus Rohrbach, Shuicheng Yan, and Jiashi Feng. Drop an octave: Reducing spatial redundancy in convolutional neural networks with octave convolution. In *Proceedings of the IEEE/CVF International Conference on Computer Vision*, pages 3435–3444, 2019. 3

[4] Sungik Choi and Sae-Young Chung. Novelty detection via blurring. *arXiv preprint arXiv:1911.11943*, 2019. 1

[5] Mircea Cimpoi, Subhransu Maji, Iasonas Kokkinos, Sammy Mohamed, and Andrea Vedaldi. Describing textures in the wild. In *Proceedings of the IEEE conference on computer vision and pattern recognition*, pages 3606–3613, 2014. 5, 7, 9

[6] Jia Deng, Wei Dong, Richard Socher, Li-Jia Li, Kai Li, and Li Fei-Fei. Imagenet: A large-scale hierarchical image database. In *2009 IEEE conference on computer vision and pattern recognition*, pages 248–255. Ieee, 2009. 1, 3, 6, 7, 9

[7] Russell L DeValois, Karen K De Valois, and Karen K DeValois. *Spatial vision*. Number 14. Oxford University Press on Demand, 1990. 3

[8] Alexey Dosovitskiy, Lucas Beyer, Alexander Kolesnikov, Dirk Weissenborn, Xiaohua Zhai, Thomas Unterthiner, Mostafa Dehghani, Matthias Minderer, Georg Heigold, Sylvain Gelly, et al. An image is worth 16x16 words: Transformers for image recognition at scale. *arXiv preprint arXiv:2010.11929*, 2020. 2, 3, 7

[9] Angelos Filos, Panagiotis Tigkas, Rowan McAllister, Nicholas Rhinehart, Sergey Levine, and Yarin Gal. Can autonomous vehicles identify, recover from, and adapt to distribution shifts? In *International Conference on Machine Learning*, pages 3145–3153. PMLR, 2020. 1

[10] Kaiming He, Xiangyu Zhang, Shaoqing Ren, and Jian Sun. Deep residual learning for image recognition. In *Proceedings of the IEEE conference on computer vision and pattern recognition*, pages 770–778, 2016. 2, 3, 7, 8

[11] Matthias Hein, Maksym Andriushchenko, and Julian Bitterwolf. Why relu networks yield high-confidence predictions far away from the training data and how to mitigate the problem. In *Proceedings of the IEEE/CVF Conference on Computer Vision and Pattern Recognition*, pages 41–50, 2019. 1

[12] Dan Hendrycks and Kevin Gimpel. A baseline for detecting misclassified and out-of-distribution examples in neural networks. *arXiv preprint arXiv:1610.02136*, 2016. 1, 2, 3, 5, 7

[13] Yen-Chang Hsu, Yilin Shen, Hongxia Jin, and Zsolt Kira. Generalized odin: Detecting out-of-distribution image without learning from out-of-distribution data. In *Proceedings of the IEEE/CVF Conference on Computer Vision and Pattern Recognition*, pages 10951–10960, 2020. 1

[14] Gao Huang, Zhuang Liu, Laurens Van Der Maaten, and Kilian Q Weinberger. Densely connected convolutional networks. In *Proceedings of the IEEE conference on computer vision and pattern recognition*, pages 4700–4708, 2017. 3

[15] Rui Huang and Yixuan Li. Mos: Towards scaling out-of-distribution detection for large semantic space. In *Proceedings of the IEEE/CVF Conference on Computer Vision and Pattern Recognition*, pages 8710–8719, 2021. 1

[16] Shiyu Liang, Yixuan Li, and Rayadurgam Srikant. Enhancing the reliability of out-of-distribution image detection in neural networks. *arXiv preprint arXiv:1706.02690*, 2017. 1, 2, 3, 5, 7

[17] Weitang Liu, Xiaoyun Wang, John Owens, and Yixuan Li. Energy-based out-of-distribution detection. *Advances in Neural Information Processing Systems*, 33:21464–21475, 2020. 1, 2, 3, 5, 7

[18] Mohammed Bany Muhammad and Mohammed Yeasin. Eigen-cam: Class activation map using principal components. In *2020 International Joint Conference on Neural Networks (IJCNN)*, pages 1–7. IEEE, 2020. 8

[19] Anh Nguyen, Jason Yosinski, and Jeff Clune. Deep neural networks are easily fooled: High confidence predictions for unrecognizable images. In *Proceedings of the IEEE conference on computer vision and pattern recognition*, pages 427–436, 2015. 1

[20] Olaf Ronneberger, Philipp Fischer, and Thomas Brox. U-net: Convolutional networks for biomedical image segmentation. In *International Conference on Medical image computing and computer-assisted intervention*, pages 234–241. Springer, 2015. 3

[21] Chenyang Si, Weihao Yu, Pan Zhou, Yichen Zhou, Xinchao Wang, and Shuicheng Yan. Inception transformer. *arXiv preprint arXiv:2205.12956*, 2022. 3

[22] Yiyou Sun, Chuan Guo, and Yixuan Li. React: Out-of-distribution detection with rectified activations. *Advances in*

Neural Information Processing Systems, 34, 2021. 1, 2, 3, 5, 7

[23] Sunil Thulasidasan, Gopinath Chennupati, Jeff A Bilmes, Tanmoy Bhattacharya, and Sarah Michalak. On mixup training: Improved calibration and predictive uncertainty for deep neural networks. *Advances in Neural Information Processing Systems*, 32, 2019. 1

[24] Laurens Van der Maaten and Geoffrey Hinton. Visualizing data using t-sne. *Journal of machine learning research*, 9(11), 2008. 9

[25] Grant Van Horn, Oisin Mac Aodha, Yang Song, Yin Cui, Chen Sun, Alex Shepard, Hartwig Adam, Pietro Perona, and Serge Belongie. The inaturalist species classification and detection dataset. In *Proceedings of the IEEE conference on computer vision and pattern recognition*, pages 8769–8778, 2018. 1, 3, 5, 6, 7, 9

[26] Ashish Vaswani, Noam Shazeer, Niki Parmar, Jakob Uszkoreit, Llion Jones, Aidan N Gomez, Łukasz Kaiser, and Illia Polosukhin. Attention is all you need. *Advances in neural information processing systems*, 30, 2017. 3

[27] Haohan Wang, Xindi Wu, Zeyi Huang, and Eric P Xing. High-frequency component helps explain the generalization of convolutional neural networks. In *Proceedings of the IEEE/CVF Conference on Computer Vision and Pattern Recognition*, pages 8684–8694, 2020. 3, 4, 6

[28] Jianxiong Xiao, James Hays, Krista A Ehinger, Aude Oliva, and Antonio Torralba. Sun database: Large-scale scene recognition from abbey to zoo. In *2010 IEEE computer society conference on computer vision and pattern recognition*, pages 3485–3492. IEEE, 2010. 5, 7, 9

[29] Bolei Zhou, Agata Lapedriza, Aditya Khosla, Aude Oliva, and Antonio Torralba. Places: A 10 million image database for scene recognition. *IEEE transactions on pattern analysis and machine intelligence*, 40(6):1452–1464, 2017. 5, 7, 9